IEEE Access
Multidisciplinary | Rapid Review | Open Access Journal

Received April 25, 2019, accepted May 23, 2019, date of publication May 30, 2019, date of current version June 13, 2019.

Digital Object Identifier 10.1109/ACCESS.2019.2920053

A Novel Fault Detection and Location Method for PV Arrays Based on Frequency Analysis

PERLA-YAZMÍN SEVILLA-CAMACHO[1,2], MARCO-ANTONIO ZUÑIGA-REYES[2,3], JOSE-BILLERMAN ROBLES-OCAMPO[2,4], ROGER CASTILLO-PALOMERA[2,4], JESÚS MUÑIZ[5], AND JUVENAL RODRÍGUEZ-RESÉNDIZ[6], (Senior Member, IEEE)

[1]Department of Mechatronic Engineering, Universidad Politécnica de Chiapas, Suchiapa 29150, Mexico
[2]Renewable Energy Postgraduate Program, Universidad Politécnica de Chiapas, Suchiapa 29150, Mexico
[3]Electric and Electronic Engineering Department, Tecnológico Nacional de México en Tuxtla Gutiérrez, Tuxtla Gutiérrez 29050, Mexico
[4]Department of Energy Engineering, Universidad Politécnica de Chiapas, Suchiapa 29150, Mexico
[5]Renewable Energy Institute, Universidad Nacional Autónoma de México, Temixco 62580, Mexico
[6]Faculty of Engineering, Universidad Autónoma de Querétaro, Santiago de Querétaro 76010, Mexico

Corresponding author: Juvenal Rodríguez-Reséndiz (juvenal@uaq.edu.mx)

This work was supported in part by the PRODEP and in part by the CONACyT under Grant 258644 and Grant 270810.

ABSTRACT This paper presents a fault detection and location method for photovoltaic (PV) arrays. One novelty of the method is the use of the different amplitude changes of the alternating current frequency component of the PV array output voltage. Another novelty is the technique used to generate the PV array output voltage. In this technique, the entire PV array is operated under dark conditions with red pulsed light only applied on one module of the PV array. Under these conditions, the presence of an open circuit fault and the variability in module impedances generate different increases in the total dynamic impedances of the PV array. As a consequence of these increases, the spectral component of the alternating current array output voltage also undergoes different increases, which facilitates fault detection. The discrete Fourier transform and statistical techniques are used to feature extraction and classification indication. The proposed method takes into account reliability and detection time and does not require the use of expensive or specialized equipment or the disconnection of or any modification to the PV array, which reduces the cost of the system. The earlier mentioned is achieved with the use of a pulsed light, which inputs a forward bias voltage into the array. The results of both the simulation and the experiment are presented in order to demonstrate the 100% effectiveness of the proposed method under different temperatures and PV array sizes.

INDEX TERMS Renewable energy, PV array fault location, dynamic impedance, open circuit fault, pulsed light signal, spectral analysis.

I. INTRODUCTION

Accelerated economic growth has resulted in the excessive use of fossil and nuclear fuels. Consequently, this has raised serious environmental concerns and has depleted resources, making the investigation of the potential of renewable energy sources vitally important. These sources must be clean and must have unlimited potential and a much lower environmental impact than other conventional energy technologies. There are three main renewable energy sources: wind, biomass, and solar.

Although rapid and continuous progress has been made in increasing efficiency and reducing the cost of photovoltaic (PV) electric power generation, the array-level management of PV installations remains much the same as that used in previous decades. The family of technologies and protocols collectively known as the smart grid offer an opportunity to change this, with significant improvements in overall array power production possible via increased monitoring and communication among PV array components [1]. If not detected and corrected quickly, faults in any components of a PV system can seriously affect the efficiency and energy yield as well as the security and reliability of the entire PV plant. In addition, persistent faults can be a fire risk. Fault detection and diagnosis (FDD) methods are indispensable for system reliability, high efficiency operation, and PV plant safety [2]. The most common failures occurring in PV arrays (PVA) are ground faults, line-to-line faults, hot spot formation, polarity mismatch, open faults, short faults, bypass diode failure, dust/soil formation in a PV array, and arc faults [3].

The associate editor coordinating the review of this manuscript and approving it for publication was Bora Onat.

Several FDD methods have been proposed in the literature, characterized by the following main features: rapid detection of malfunctions; complexity and sensors requirements; required climatic and electrical input data; and, selectivity (i.e. the ability to distinguish between different faults). Said faults can be globally classified into two main categories [4], visual-thermal and electrical, of which, the use of electrical signatures is a more promising and advantageous option for monitoring and diagnostic systems [5]. Electrical methods can be classified into five groups [6]: statistical and signal processing approaches; the analysis of I-V characteristics; power loss analysis; voltage and current measurement; and, artificial intelligence techniques. These methods are used for the detection and diagnosis of different type of faults. Some methods can detect, localize and classify possible faults occurring in a PVA, while other methods only perform one or two of these actions. This is due to the technique used and the features of the analyzed failure.

Several methods have been reported in the literature that detects or/and identifies the open circuit failure (OCF). In [7], a procedure to the prediction of PV behavior under any environmental condition is proposed. The method is based on both descriptive and inferential statistics for the diagnosis of PV plants. The PV plant will be considered to be composed of k identical sub-arrays, each of them being equipped with a unit of measurement. In [8], a fault diagnosis meter based on extension neural network (ENN) is presented. In this method, I-V and P-V curves, the maximum output power, voltage of maximum power point, current of maximum power point, open circuit voltage, temperature and irradiance of the PV array are required. In another study [9], the number of open and short circuit faults is detected. This method is based on the measurement of the operating voltage of PV string and ambient temperature. Moreover, a method based in 3-Sigma rule, Hampel identifier, and Boxplot rule is presented to detect the presence of open string. In this method, two reference modules, a voltage and a current sensor for each string is required [10]. Graph-based semi-supervised learning model is also proposed to detect and identifies the possible fault type. For that, PV array voltage, array current, solar irradiance, PV operating temperature, and references modules are required [11]. In [12], the fault detection is based on time series of PV string current. In [13], [14], an innovative model-based fault-detection approach for early detection of shading of PV modules and faults on the direct current (DC) side of PV systems is proposed. This approach combines the flexibility and simplicity of a one-diode model with the extended capacity of an exponentially weighted moving average (EWMA) control chart to detect incipient changes. In [15], a simple diagnostic method to determine the number of open and short-circuited PV modules in a string of a PV system is proposed. Temperature and irradiance sensors, as well as a power meter by string are needed. Mini PV modules are used in a portable PV array. In [16], a voltage based protection scheme that detects classifies and locates string to-ground, string-to-string, and open-circuit faults in utility-scale PV arrays is presented. However, the location is only for a fault of string to-ground and string-to-string. The protection scheme operates based on the magnitude and wave-shape properties of voltage signals. Two voltage sensors are required for each string of the PV array. Furthermore, a fault detection scheme based on monitoring the output power of the PV array is presented. Using the sample entropy-based complexity, the irregularity of the time series of the normalized fault-imposed component of PV power is quantified as the fault detection criterion. The proposed protection scheme is capable of distinguishing the line-to-line, line-to-ground, and open-circuit faults from the weather disturbances and partial shadings [17]. However, in order to make the faults more easily to be eliminated, it is essential to locate the fault PV string or module. There are a few PV array open circuit fault location methods. In [18]–[20], the Time Domain Reflectometry (TDR) has been used for location and identification of open and short circuit in PV module string. This technique also has been used for a large size PV plant in operating conditions. However, only the diagnostic monitoring is carried out [21]. In [22], a disconnection detection and location method using an earth capacitance measurement (ECM) in PV module string was experimentally studied. The method is sensorless, but an LCR meter is required. In [23], two methods for the fault location in PV module string were experimentally studied. One was the ECM and the other was the TDR.

In all the location methods mentioned above, the methods operate under dark conditions, offline and disconnection of each string is required for a series-parallel configuration, which results in less productivity for modification to the PV array; and an increase in the costs due to the disconnection, and the individual and manual testing of each string. In addition, the safety of the maintenance personnel is not ensured.

An overview of some of the PV array fault detection and location methods reported show that the methods present both advantages and limitations in terms of approach, sensor requirements, the ability to diagnose and locate faults, integration complexity, accuracy, applicability, experimental validation, and implementation cost.

In addition, these methods only analyze the direct current (DC) response of the PVA, and neglect the analysis of the alternating current (AC) response. However, the AC signal of the PV array output voltage provides important information that can be digitally processed using spectral and statistical methods in order to extract important information that facilitates fault detection. Spectral analysis is used extensively for condition monitoring and fault diagnostics in electrical, mechanical and electromechanical systems [24], [25]. However, spectral analysis has only been used to detect arc faults in monitoring PV systems [26].

The main objective of the present research is to develop a novel method based on spectral analysis for detecting and locating only OCF in a string of a PVA. Unlike existing methods, it is easily implemented, has been applied and verified experimentally on different scale PV plants, and operates

at low-cost. The estimated implementation cost is approximately USD 1000. Moreover, it does not require expensive or specialized equipment, nor does it require the disconnection of or any modification to the PV array. The method proposed uses the Discrete Fourier Transform (DFT) and a classifier based on statistical techniques.

The innovation of the method is its simplicity, low-cost and low computing power compared to other reported FDI techniques. In addition, this proposed method not only detects an open circuit fault but also locates the failure string, which is a novelty in comparison with other methods that analyzed the same fault.

The main novelty of the method is its use of the different amplitude changes of the AC frequency component of the PV array output voltage. These amplitude changes are caused by the changes in the total dynamic impedances of the array as a result of open string fault and variability in module impedances. For this reason, the entire array is operated in dark conditions with the pulsed light only applied on one module of the PV array. Experimental and simulated tests were carried out to demonstrate and validate the proposed method. Various temperatures and various array sizes were considered.

The proposed method can detect and locate only open circuit fault in one string in a PV array. However, the partial shading or cloud cover do not generate a false alarm. This is due to the entire PV array is operated under dark condition, and the presence of these faults does not lead to significant changes on the AC parameters of the array.

The paper is organized as follows: the modeling of a PV array is presented in Section II. The basic structure of the proposed fault location method is provided in Section III. A brief description of the DFT technique is presented in Section IV. Section V presents the feature extraction technique. Section VI describes the classifier and indicator based on statistical analysis. Section VII describes the experimental validation of the proposed method. Finally, Sections VIII and IX provide an analysis of the data and the fault location results, and the study's conclusions, respectively.

II. MODELING OF A PV MODULE AND ARRAY

A photovoltaic module can be represented with its single-diode equivalent circuit, as shown in Fig. 1. In [29], the relationship between output current and voltage is given by the following nonlinear equation:

$$I = I_{ph} - I_o\left(\exp\left(\frac{q\,(V + IR_s)}{nkT}\right) - 1\right) - \frac{V + IR_S}{R_{sh}} \qquad (1)$$

where I_{ph} is the light-generated photocurrent,I_O is the reverse saturation current of the diode, q is the electron charge, n is the ideality factor for a p-n junction, k is the Boltzman constant, T is the temperature of the module, R_S is the series resistance, R_{sh} is the shunt resistance, and I and V, respectively, are the current and voltage outputs of the module.

The I–V characteristics of solar cells measured under both dark and illuminated conditions provide an important tool for assessing their performance. In some reported studies [30], the cells or modules are tested in dark conditions in order to characterize their dynamic impedance. In these studies, a sinusoidal or square wave with varying frequencies is input into the solar cell in either forward or reverse bias. The results are obtained in the following ways: 1) The impedance loci are plotted and interpreted in complex plane at any bias level; and, 2) The responses are calculated by applying signal processing to the input and output signals, using Fast Fourier Transform (FFT) techniques to obtain the various harmonic contents of the input and output.

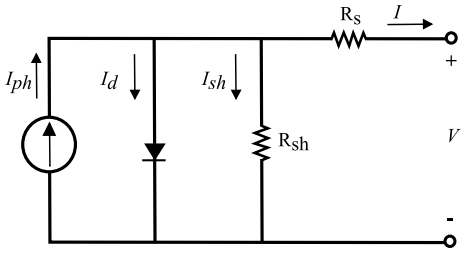

FIGURE 1. Electrical equivalent circuit of the photovoltaic cell.

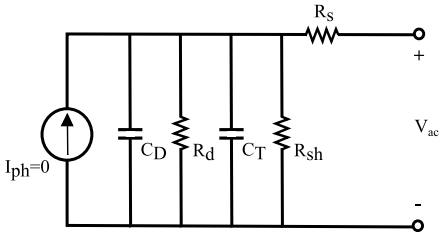

FIGURE 2. AC equivalent circuit of a PV module.

Fig. 2 shows the AC equivalent circuit of a solar cell, without a light-generated current, the dynamic impedance of which is measured and derived under these conditions.

Under dark conditions when looking into the solar cell output port, the solar cell impedance $Z_{PV}(\omega)$ at a frequency ω can be shown to consist of one resistive component and one reactive component. At each bias voltage V, the impedance $Z_{PV}(\omega)$ can be expressed as the equation:

$$Z_{PV}\,(V, \omega) = R_{PV}\,(V, \omega) + jX_{PV}\,(V, \omega) \qquad (2)$$

For simplicity, V is removed of (2) and written as follows:

$$Z_{PV}\,(\omega) = R_{PV}\,(\omega) + jX_{PV}\,(\omega)$$
$$Z_{PV} = \left[R_S + \frac{R_p}{\left(\omega R_p C_p\right)^2 + 1}\right] - j\left[\frac{\omega R_p^2 C_p}{\left(\omega R_p C_p\right)^2 + 1}\right] \qquad (3)$$

where R_p is the parallel resistance of R_{sh} and R_d, and C_P is the parallel capacitance of C_D and C_T.

The application of frequency domain analysis to a PV cell or modules under dark conditions can be used not only to obtain their dynamic parameters but also to detect failures in a PV array. A PV array is constructed by connecting a number of modules in both series and parallel. If the entire PV

array operates under illuminated conditions, the short circuit current and maximum power decrease due to open circuit fault, while the open voltage stays close to its normal value. However, if the entire PV array is tested under dark conditions and only one PV module in the array is illuminated with a pulsing light to generate a pulsing output voltage, as shown in Fig. 3 (voltage to be applied to the other modules), then the presence of OCF generates an increase in the dynamic impedance of the array (Z_{ary}). The reason of this increase is due to the PV strings (impedances) on the PV array are connected in a parallel circuit.

$$Z_{ary} = \frac{1}{\frac{1}{Z_A} + \frac{1}{Z_B} + \frac{1}{Z_C} + \frac{1}{Z_D}} \tag{4}$$

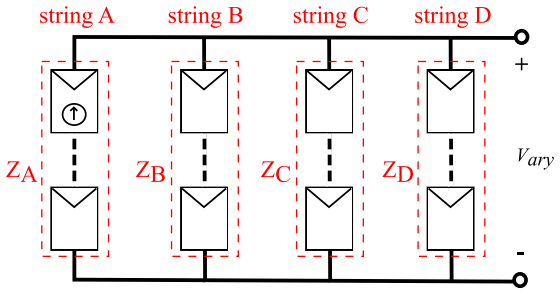

FIGURE 3. PV array in serial-parallel configuration.

An increase in the total impedance generates an increase in the array output voltage, due to the fact that the current$I$, obtained from the illuminated module, is constant. Using the AC equivalent circuit of the array, the PV array voltage equation is given by:

$$V_{ary}(\omega) = I(\omega) Z_{ary}(\omega) \tag{5}$$

The disconnection (open circuit failure) presented by each of the strings generates different output voltage values for the array due to the variability in module impedances [31]. Therefore, the differences in the output voltage values enable the detection and location of the string with an open circuit fault in a series-parallel PV array.

III. OPEN CIRCUIT FAULT LOCATION ALGORITHM

The method is designed to describe the operation of a PV array under dark conditions with the application of a pulsed light on one module of the farthest string from a PV array. For the signal generation, various frequencies were tested experimentally. In all the tests, the method demonstrated to be effective. The only condition is that this frequency was much higher than the frequency of 60 Hz. This avoids interference with the signals of the power supply. In this research, the frequency used is of 6 kHz.

The use of pulsed light inputs a forward bias voltage into the array without requiring either the disconnection of or any modification to the PV array.

The amplitudes of the frequency component at 6 kHz are analyzed to locate an open circuit fault in a string. Changes in the amplitude of this frequency are generated due to changes in the total impedance of the array (using (5)), which is a result of the disconnection (using (4)) and variability of the impedances presented by each of the strings in the array [31]. Based on these changes, DFT can be used to extract important information that facilitates the identification of a fault position. In this respect, the AC component of the PV array output voltage is measured, processed and analyzed. A diagram of the proposed model is depicted in Fig. 4.

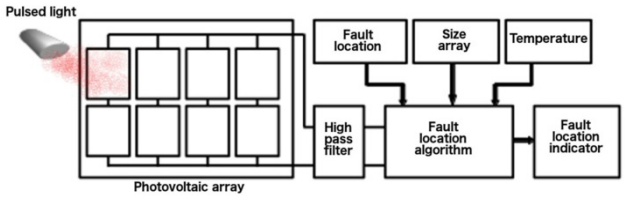

FIGURE 4. Fault location system.

The method operates in two modes, learning and monitoring, in both of which the pulsed light is applied under dark conditions. The light is generated by a high power red light source. This particular light source was chosen because this color light has been shown to be more effective when it is incident on a solar cell [27]. The temperature, array size and fault location are required for the learning operation mode, whereas only the temperature and size array are required for the monitoring mode. An algorithm was developed to locate the OCF in the strings of the PV arrays. The flowchart for the proposed algorithm is presented in Fig. 5, with the step-by-step explanation of the algorithm set out below.

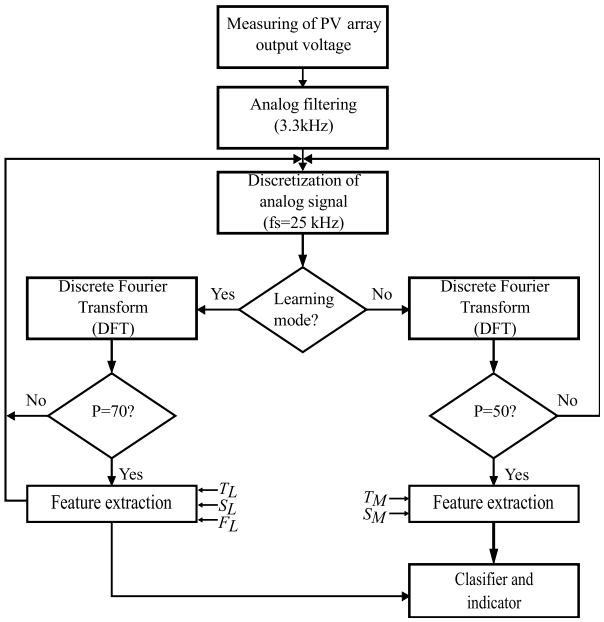

FIGURE 5. Flowchart for the fault location algorithm.

Once the module has been lit, the PV array output voltage (V_{ary}) is measured and filtered ($x(t)$) to eliminate some

frequencies, 0 Hz and 60 Hz, which are the DC frequency component and the AC frequency component of the supply line, respectively. The filter also eliminates other spurious frequencies. The presence of these additional frequency components interferes with the detection of the condition of the string. For this reason, prior to the acquisition of the data, the output voltage is conditioned using an analog filter composed of a passive high pass *RC* filter with a cut-off frequency (f_c) defined within the range of 60 Hz and 6 kHz, which is the frequency of the pulsed light, as shown in Fig. 6 (a).

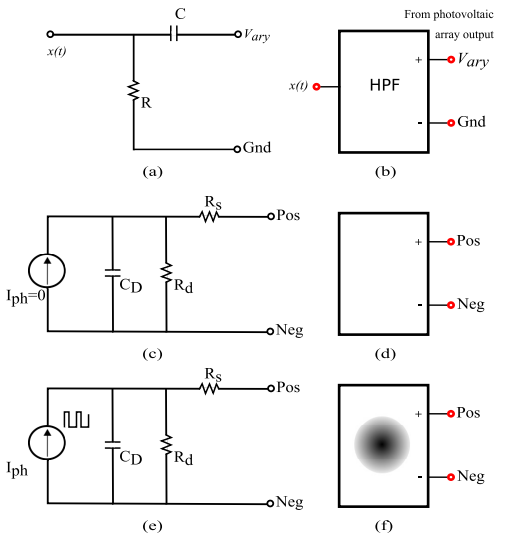

FIGURE 6. (a) Passive high pass RC filter, (b) symbol for the circuit schematic of the RC filter, (c) AC equivalent circuit of a solar cell used for simulation, (d) symbol for the circuit schematic of a solar cell, (e) AC equivalent circuit of a solar cell with signal generator, and (f) symbol of the circuit schematic or solar cell with signal generator.

This filter passes only those signal frequencies that are higher than the f_c and rejects frequencies that are lower than the f_c, meaning that the filter eliminates those frequencies that are below the frequency of the pulsed light. The filter design is based on the following:

$$R = \frac{1}{2\pi f_c C} \tag{6}$$

where R is a resistor and C is a capacitor with a given value.

One period ($x(t,p)$) of the filtered time-domain signal ($x(t)$) is then discretized ($x(r,p)$) and transformed into a frequency domain via DFT technique ($X(d,p)$), as is depicted in Section IV. The Fourier coefficients of the induced frequency are obtained from this process, which is conducted for several acquired periods, while the median of the magnitudes of the Fourier coefficients for the induced frequency is calculated for all acquired periods.

The median obtained gives a different value for each fault location and is used as an input data vector of both a classifier and indicator. The output of the statistical classifier gives the exact location of the open circuit string.

As the signal processing is digital and the filtered signal is analog, an analog to digital data conversion is required prior to the acquisition, the signal for which is sampled at a frequency of 25 kHz. This frequency was chosen according to the Nyquist sampling theorem, which stipulates that the sampling frequency (f_s) must be at least twice the highest analog frequency component, which is 6 kHz.

IV. DIGITAL SIGNAL PROCESSING

A faster version of the Discrete Fourier Transform (DFT), the FFT is a signal processing technique which transforms a signal from the time domain to the frequency domain, facilitating frequency (spectrum) analysis. The spectral representation of a time signal is, therefore, a collection of AC and DC components in the frequency domain, each with a specific frequency, amplitude and phase angle [24]. As the analysis aims to find a simple and effective transform for the original signals, the important information contained in the signals can be shown and the dominant features of the signals can then be extracted for fault diagnosis.

Taking a period of the input signal $x(t,p)$, which is filtered and discretized in order to obtain the signal $x(r,p)$, where integer variable r refers to the sample number of a discrete series and p is the number of acquired periods, the DFT of the sampled input sequences, $x(r,p)$, is defined by (7).

$$X(d,p) = \left[\sum_{r=0}^{N-1} x(r,p)\, e^{\frac{-2\pi i}{N} dr}\right]_{p=1}^{P} \tag{7}$$

Here, d is used to denote the frequency domain ordinal, while$N$ is the length of the sequence to be transformed, and P is the length of acquired periods. The digital processing requires the number of samples acquired for each period to be a power of two. Furthermore, the number of acquired periods for the learning operation mode must be greater than those acquired for the monitoring mode.

In order to evaluate the fault location using DFT signal processing, a PV array output voltage signal was constructed to simulate the location of strings with an open circuit fault in the PV arrays. The simulation was applied using PV arrays comprising 4×1 and 4×2 PV modules, which were connected in a series-parallel configuration. The open circuit fault presented 5 locations: any string; String A; String B; String C; and, String D. The simulations were carried out on a Quite Universal Circuit Simulator (QUCS). The AC equivalent circuit of a solar cell, as used in this research and its schematic circuit symbols are shown in Fig. 6 (c) and (d), respectively. This circuit is the AC circuit presented in Fig. 2, but R_{sh} and C_T were eliminated from the original circuit due to the operating conditions. The values for the remaining elements were taken into account, depending on the characteristics of the module simulated. In previous studies [28], these values were obtained for solar cells operating under various conditions and comprising a voltage of 0.6 volts, a solar radiance of 0 W/m^2, an $I_{ph} = 0$ A, and temperatures ranging from 22 and 25°C. Under these conditions, an $R_d = 0.112\Omega$, a $C_D = 450\mu$F and an $R_s = 0.045\Omega$ were obtained.

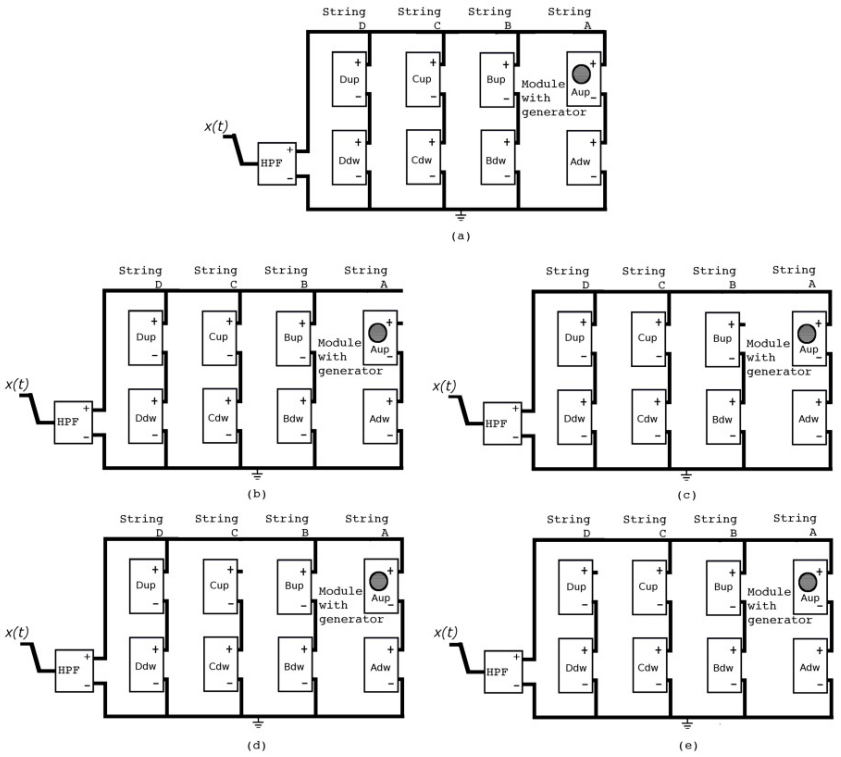

FIGURE 7. Circuit schematic of the 4 × 2 PV array simulated with different open circuit locations: (a) any string, (b) in String A, (c) in String B, (d) in String C, and (e) in String D.

The pulsed light signal was simulated by means of a squared signal with a frequency of 6 kHz. A signal generator was connected in a series with one of the AC equivalent circuits of the solar cell in order to generate the simulated light signal, as shown in Fig. 6 (e). The circuit schematic symbol for a module used with a pulsed light is shown in Fig. 6 (f).

Fig. 6 (b) shows the schematic symbol for the high pass filter at an f_c of 3.3 kHz.

Fig. 7 shows the circuit schematic of the simulated 4 × 2 PV array.

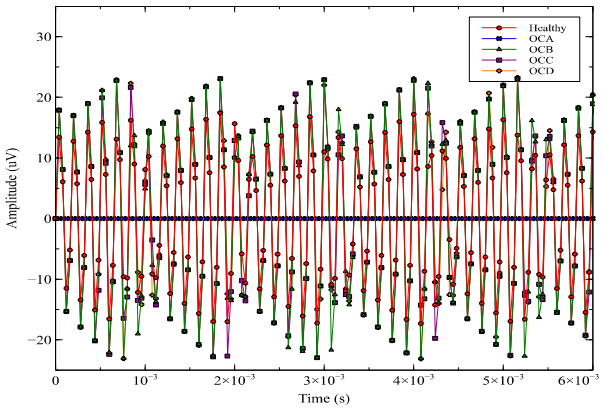

FIGURE 8. Output voltage of the 4 × 2 PV array simulated with 5 open circuit locations.

Fig. 8 was created in order to compare the output voltages for the 5 open circuit fault locations. The voltage was obtained

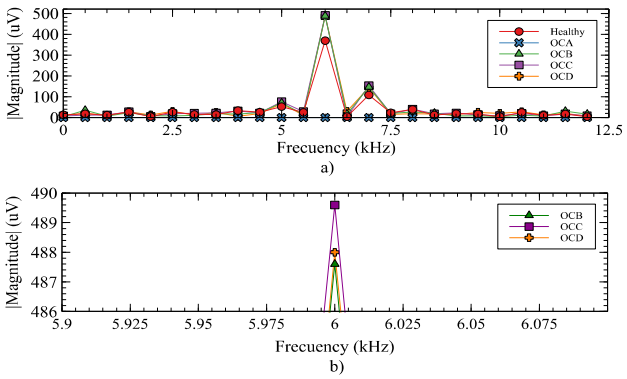

FIGURE 9. DFT spectrum of the AC component output voltage obtained from the simulated 4 × 2 PV array.

in the simulated 4 × 2 PV array, from which segments of 64 samples were collected, corresponding to a window length of 0.00256 s at an f_S of 25 kHz. As can be seen in Fig. 8, the signal in the time domain does not offer enough information regarding the string condition in order to locate its open circuit fault. In order to solve this situation, the DFT is applied to the signals detailed in Fig. 8. The DFT power spectrums of the AC component of these signals are shown in Fig. 9, while the DFT analysis shows that dominant peak frequency occurs at 6 kHz, which is the frequency of the simulated light. Comparing the power amplitudes at this frequency reveals that the lowest amplitude is obtained in the PV array that did not fail. A magnification of the power amplitudes, obtained

from the PV array with OCF, shows an amplitude difference among each of the possible PV arrays with OCF in a string. These differences enable the proposed method to detect the PV array condition and locate the string via OCF.

In order to demonstrate the scalability of the proposed method, a PV array of 20 × 5 modules was simulated. The simulation was performed with the same conditions mentioned for the 4 × 1 and 4 × 2 PV arrays. In this test, the method also demonstrates 100% effectiveness. The DFT power spectrums of the AC component of these signals are shown in Fig. 10.

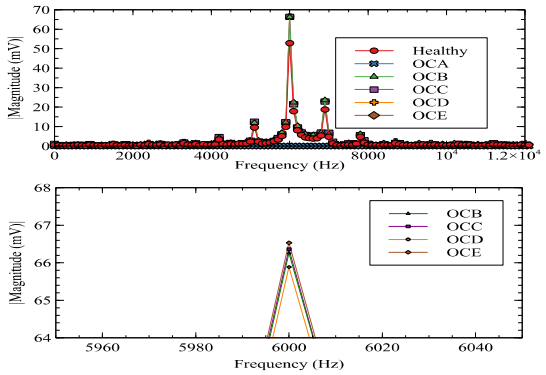

FIGURE 10. DFT spectrum of the AC component output voltage obtained from the simulated 20 × 5 PV array.

Fig. 10 shows that for the 5 open circuit fault location, the dominant peak frequency occurs at 6 kHz. The lowest amplitude is obtained in the PV array healthy, and there are differences in amplitude between each of the possible open circuit failure locations. These characteristics are similar to the obtained for the 4 × 2 PV array. This demonstrates the 100% effectiveness of the proposed method under different PV array sizes.

A. SIGNAL PROCESSING FOR THE LEARNING OPERATION MODE

In order to identify the fault locations of the open circuit strings in PV arrays, the system must first be trained. The training consists of obtaining a database, for each PV array analyzed, which contains the reference values of the PV array. This requires that the digital signal processing (see (7)) is carried out for various conditions of temperature (T_L), open circuit failure location (F_L), and size of the PV array (S_L). In this learning mode, 70 signal periods are acquired for 64 samples. The number of required signal periods and samples had already been obtained experimentally. Once the signal processing is complete, the feature extraction is carried out, as is depicted in Section V.

This training is a highlighted process of the proposed method. This is due to the fact that each photovoltaic module of the array has a high dispersion and variability of its AC parameters [31]. And the particular characteristics of each PV array needs be obtained, and stored in a database. In addition, this training allows to adjust the reference value according to the current conditions. For example, the aged can change the AC parameters of PV modules. In this work, the PV array is not aged. Nevertheless, if the whole PV array is aged, this aged is not a significant factor for the proposed method because reference value will be changed according to the current conditions.

B. SIGNAL PROCESSING FOR THE MONITORING OPERATION MODE

After the system has been trained, as is depicted in Sections IV A and V, the PV arrays are monitored by first applying the digital signal processing (see (7)). Then the feature extraction process depicted in section V. In this monitoring mode, 50 signal periods are acquired for 64 samples and the temperature (T_M) is monitored, while the user enters the size array (S_M) into the system. The number of signal periods was set to 50, because it satisfies the minimum sample size for using a nonparametric statistical test.

V. FEATURE EXTRACTION

The median value of the Fourier coefficients corresponding to a 6 kHz frequency is obtained, taking into account the DFT results (see (8)). The magnitude of these Fourier coefficients is extracted from the matrix $X(d,p)$ and stored in an array $Y(p)$.

$$\tilde{X} = \frac{1}{2}\left[Y\left(\frac{p}{2}\right) + Y\left(\frac{p}{2}+1\right)\right] \tag{8}$$

As the feature extraction process is applied to two operation modes, two arrays are required to store the median values obtained. For the learning mode, the median values are stored in an array with identifiers $L(T_L, S_L, F_L)$, whereas, for the monitoring mode, the median value is stored in a variable $M(T_M, S_M)$.

VI. CLASSIFIER AND INDICATOR

In this study, fault location is based on the lowest value obtained from the squares of the differences among the median reference values $L(T_L, S_L, F_L)$ and the median value of the monitoring operation mode $M(T_M, S_M)$. This last median value is only subtracted from those pre-calculated reference values that have the same temperature range (T_M) and the same PV array size (S_M) as the test.

$$J(F) = \left(L(T_L, S_L, F_L) - M(T_M, S_M)\right)^2 \Big|_{F_L=0}^{4} \tag{9}$$

The F value pertaining to the lowest value of $J(F)$ enables the detection of the PV array condition. If an open circuit fault is detected in a string, its location is indicated to the user on the computer screen.

Due to the low dispersion characteristics of the PV array response to open circuit failure conditions in the strings, no more sophisticated classification techniques are required, which would only add complexity to the method

VII. VALIDATION OF THE PROPOSED METHOD

A. EXPERIMENTAL SETUP

The temperature was measured with a digital thermometer 6300699 (RadioShack^R). Moreover, 8 polycrystalline

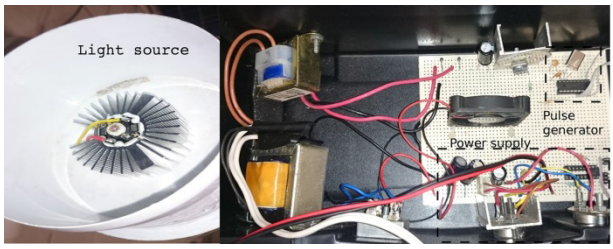

FIGURE 11. Experimental setup.

silicon modules (50 W/module) were connected with a 12 American Wire Gauge (AWG). The experimental setup is shown in Fig. 11. The pulsed light system contains two DC power suppliers, a pulse generator, and a light source, as shown in Fig. 12. The latter comprises a heat sink and a red light-emitting 5-watt diode (LED) pulsed at a frequency of 6 kHz. This frequency is controlled by the pulse generator, which is designed with an 8-bit Microchip microcontroller.

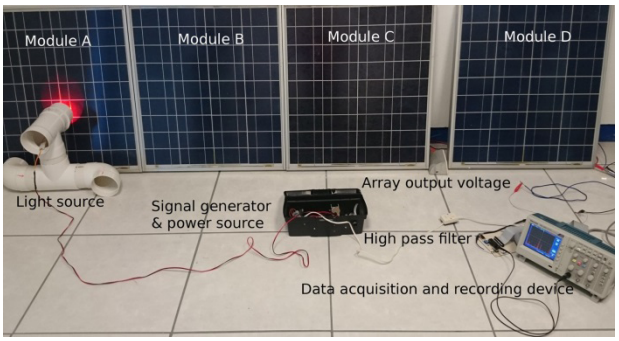

FIGURE 12. Pulsed light system.

The AC component of the PV array output voltage was acquired and recorded using a two-channel oscilloscope TBS 1042 (Tektronik^{TM}).

Segments corresponding to a window length of 0.00256 s at a sampling frequency of 25 kHz were collected from 64 samples. The collected samples were processed and analyzed with PYTHON^{TM}, while the NumPy package and the CSV module were also used. Prior to the acquisition and processing of the data, this signal was filtered.

To verify the efficiency of each solar PV module, the short-circuit current (I_{sc}) and the open-circuit voltage (V_{oc}) were measured at a solar radiance of 200 W/m^2 and a temperature of 25°C. Additionally, each PV module was lit with a pulsed light of 6 kHz, while the spectral component at 6 kHz ($X(15,1)$) was obtained using the DFT.

B. EXPERIMENTAL PROCEDURE

In order to test its effectiveness, the proposed method is applied across 30 different case studies under the conditions described below. PV arrays comprising 4 × 1 and 4 × 2 PV modules were connected in a series-parallel configuration. The signal processing for the learning operation mode was carried out for 3 temperatures (T_L), 5 open circuit failure locations (F_L), and 2 different-sized PV arrays (S_L). The resulting 30 median values are stored in an array with the identifiers $L(T_L, S_L, F_L)$, see Table 1. The open circuit fault presented in 5 locations: any string; String A; String B; String C; and, String D.

TABLE 1. Database identifiers for different temperatures (TL), size array (SL) and failure location (FL).

Database identifier $L(T_L,S_L,F_L)$	Temperature (T_L) (°C)	Size array (S_L)	Failure location (F_L)
$L(1,1,0)$	1 (23 to 25)	1 (4x1)	0 (No fault in array)
$L(1,1,1)$			1 (OCF in String A)
$L(1,1,2)$			2 (OCF in String B)
$L(1,1,3)$			3 (OCF in String C)
$L(1,1,4)$			4 (OCF in String D)
$L(2,1,0)$	2 (25 to 27)		0 (No fault in array)
$L(2,1,1)$			1 (OCF in String A)
$L(2,1,2)$			2 (OCF in String B)
$L(2,1,3)$			3 (OCF in String C)
$L(2,1,4)$			4 (OCF in String D)
$L(3,1,0)$	3 (27 to 29)		0 (No fault in array)
$L(3,1,1)$			1 (OCF in String A)
$L(3,1,2)$			2 (OCF in String B)
$L(3,1,3)$			3 (OCF in String C)
$L(3,1,4)$			4 (OCF in String D)
$L(1,2,0)$	1 (23 to 25)	2 (4x2)	0 (No fault in array)
$L(1,2,1)$			1 (OCF in String A)
$L(1,2,2)$			2 (OCF in String B)
$L(1,2,3)$			3 (OCF in String C)
$L(1,2,4)$			4 (OCF in String D)
$L(2,2,0)$	2 (25 to 27)		0 (No fault in array)
$L(2,2,1)$			1 (OCF in String A)
$L(2,2,2)$			2 (OCF in String B)
$L(2,2,3)$			3 (OCF in String C)
$L(2,2,4)$			4 (OCF in String D)
$L(3,2,0)$	3 (27 to 29)		0 (No fault in array)
$L(3,2,1)$			1 (OCF in String A)
$L(3,2,2)$			2 (OCF in String B)
$L(3,2,3)$			3 (OCF in String C)
$L(3,2,4)$			4 (OCF in String D)

For the signal processing required by the monitoring operation mode, test cases were generated by randomly varying the temperature test (T_M), the PV array size test (S_M), and the open circuit failure location test (F_M). The different values for each of these parameters ($3 \times 2 \times 5 = 30$ test cases) are given in Table 2. The resulting 30 median values are stored in an array with the $M(T_M, S_M, F_M)$ identifiers. For each monitoring test, 50 signal periods for 64 samples are acquired. The information from the open circuit failure location (F_M) is provided in order to ascertain the test conditions and validate the results. After the learning and monitoring data is obtained, the classifier and indicator process is then applied.

Prior to the acquisition and processing of the data, the signal was filtered through a passive high pass *RC* filter, which was designed with an f_c of 3.3 kHz and a proposed *C* of 2.2 pF, while an R of 2.2 MΩ was obtained using (6).

In order to demonstrate the scalability of the proposed method, experimental tests were carried out with the

TABLE 2. Test identifiers for different temperature tests (T_M), sizes array test (S_M) and failure location tests (F_M).

Test identifier $M(T_M,S_M,F_M)$	Temperature test (T_M) (°C)	Size array test (S_M)	Failure location test (F_M)
M(1,1,0)	1 (23 to 25)	1 (4x1)	0 (No fault in array)
M(1,1,1)			1 (OCF in String A)
M(1,1,2)			2 (OCF in String B)
M(1,1,3)			3 (OCF in String C)
M(1,1,4)			4 (OCF in String D)
M(2,1,0)	2 (25 to 27)		0 (No fault in array)
M(2,1,1)			1 (OCF in String A)
M(2,1,2)			2 (OCF in String B)
M(2,1,3)			3 (OCF in String C)
M(2,1,4)			4 (OCF in String D)
M(3,1,0)	3 (27 to 29)		0 (No fault in array)
M(3,1,1)			1 (OCF in String A)
M(3,1,2)			2 (OCF in String B)
M(3,1,3)			3 (OCF in String C)
M(3,1,4)			4 (OCF in String D)
M(1,2,0)	1 (23 to 25)	2 (4x2)	0 (No fault in array)
M(1,2,1)			1 (OCF in String A)
M(1,2,2)			2 (OCF in String B)
M(1,2,3)			3 (OCF in String C)
M(1,2,4)			4 (OCF in String D)
M(2,2,0)	2 (25 to 27)		0 (No fault in array)
M(2,2,1)			1 (OCF in String A)
M(2,2,2)			2 (OCF in String B)
M(2,2,3)			3 (OCF in String C)
M(2,2,4)			4 (OCF in String D)
M(3,2,0)	3 (27 to 29)		0 (No fault in array)
M(3,2,1)			1 (OCF in String A)
M(3,2,2)			2 (OCF in String B)
M(3,2,3)			3 (OCF in String C)
M(3,2,4)			4 (OCF in String D)

TABLE 3. Median monitoring values $M(T_M, S_M, F_M)$ and database of median reference values $L(T_L, S_L, F_L)$ of the experimental tests carried out on 4 × 1 and 4 × 2 PV arrays.

Database Identifier $L(T_L, S_L,F_L)$	Median reference value	Test identifier $M(T_M,S_M,F_M)$	Median monitoring value
L(1,1,0)	0.4293	*M(1,1,0)*	0.4522
L(1,1,1)	0.0204	*M(1,1,1)*	0.0054
L(1,1,2)	0.5707	*M(1,1,2)*	0.5764
L(1,1,3)	0.5928	*M(1,1,3)*	0.5852
L(1,1,4)	0.5223	*M(1,1,4)*	0.5088
L(2,1,0)	0.4577	*M(2,1,0)*	0.4325
L(2,1,1)	0.0209	*M(2,1,1)*	0.0051
L(2,1,2)	0.5698	*M(2,1,2)*	0.5654
L(2,1,3)	0.574	*M(2,1,3)*	0.5884
L(2,1,4)	0.5039	*M(2,1,4)*	0.5017
L(3,1,0)	0.4198	*M(3,1,0)*	0.4229
L(3,1,1)	0.0203	*M(3,1,1)*	0.0058
L(3,1,2)	0.5598	*M(3,1,2)*	0.5551
L(3,1,3)	0.5669	*M(3,1,3)*	0.577
L(3,1,4)	0.4955	*M(3,1,4)*	0.499
L(1,2,0)	0.4158	*M(1,2,0)*	0.3988
L(1,2,1)	0.0200	*M(1,2,1)*	0.0073
L(1,2,2)	0.5263	*M(1,2,2)*	0.5138
L(1,2,3)	0.451	*M(1,2,3)*	0.4547
L(1,2,4)	0.5558	*M(1,2,4)*	0.5599
L(2,2,0)	0.3799	*M(2,2,0)*	0.3873
L(2,2,1)	0.0208	*M(2,2,1)*	0.0064
L(2,2,2)	0.4997	*M(2,2,2)*	0.5051
L(2,2,3)	0.4487	*M(2,2,3)*	0.446
L(2,2,4)	0.5421	*M(2,2,4)*	0.5435
L(3,2,0)	0.3812	*M(3,2,0)*	0.3652
L(3,2,1)	0.0201	*M(3,2,1)*	0.0078
L(3,2,2)	0.4956	*M(3,2,2)*	0.5018
L(3,2,3)	0.4323	*M(3,2,3)*	0.4375
L(3,2,4)	0.5363	*M(3,2,4)*	0.5463

maximum number of PV modules available in the laboratory (12 modules). The PV array consists of 4 × 3 modules.

VIII. ANALYSIS OF EXPERIMENTAL DATA AND RESULTS

The median values for the learning mode $L(T_L,S_L,F_L)$ and the monitoring mode $M(T_M,S_M,F_M)$, obtained during the experimentation, are shown in Table 3. It shows that, in all cases, the lowest median value is obtained when the OCF is present in String A. This is due to the location of the lit module on this string, on one module of which the presence of a failure is also identified as blocking the passage of the voltage to the other strings on the PV array. The table also indicates no relationship between the median values obtained and the location of the string. This is due to the great variability in module impedances for the different modules used.

In order to demonstrate the above, each module is tested individually under the same conditions, while its I_{sc}, V_{oc} and V_{out} is also measured. The results obtained are shown in Table 4 and reveal that each module has different electrical parameters due to its different dynamic parameters. The table also shows that the PV modules identified as C_{up} and C_{dw}, shown in Fig. 6, have the greatest I_{sc} and V_{out}; however,

TABLE 4. Individual electrical characteristics of the experimental modules.

PV Module identifier	V_{oc} (V)	I_{sc} (mA)	$X_{(15,1)}$ (V)
A_{up}	15	400	0.973
A_{dw}	13.99	270	1.321
B_{up}	19.35	300	1.067
B_{dw}	14	271	0.998
C_{up}	16.99	380	2.161
C_{dw}	16.88	390	2.264
D_{up}	13.36	300	0.743
D_{dw}	13.41	250	1.125

these differences do not interfere with condition detection and failure location. In addition, Table 3 indicates that the median values obtained from the PV array without failure are lower than those obtained for the PV arrays with failure on strings B, C or D. Furthermore, results also indicate that

TABLE 5. ***J(F)*** **Values obtained from all the experimental tests conducted on the 4 × 1 PV array.**

		Database Identifier $L(T_L,S_L,F_L)$															
		L(1,1,0)	*L(1,1,1)*	*L(1,1,2)*	*L(1,1,3)*	*L(2,1,4)*	*L(2,1,0)*	*L(2,1,1)*	*L(2,1,2)*	*L(2,1,3)*	*L(2,1,4)*	*L(3,1,0)*	*L(3,1,1)*	*L(3,1,2)*	*L(3,1,3)*	*L(3,1,4)*	**Indicator of failure location**
Test identifier $M(T_M,S_M,F_M)$	*M(1,1,0)*	5.2	1864	140.4	197.6	49.1	-	-	-	-	-	-	-	-	-	-	0 (No fault in array)
	M(1,1,1)	1796	2.25	3195	3450	2671	-	-	-	-	-	-	-	-	-	-	1 (OCF in String A)
	M(1,2,2)	216.3	3091	0.3	2.6	29.2	-	-	-	-	-	-	-	-	-	-	2 (OCF in String B)
	M(1,1,3)	243	3189	2.1	0.5	39.5	-	-	-	-	-	-	-	-	-	-	3 (OCF in String C)
	M(1,2,4)	63.2	2385	38.3	70.5	1.8	-	-	-	-	-	-	-	-	-	-	4 (OCF in String D)
	M(2,1,0)	-	-	-	-	-	6.3	1694	188.5	200.2	50.9	-	-	-	-	-	0 (No fault in array)
	M(2,1,1)	-	-	-	-	-	2048	2.49	3188	3236	2488	-	-	-	-	-	1 (OCF in String A)
	M(2,1,2)	-	-	-	-	-	115.9	2964	0.1	0.7	37.8	-	-	-	-	-	2 (OCF in String B)
	M(2,1,3)	-	-	-	-	-	170.8	3220	3.4	2	71.4	-	-	-	-	-	3 (OCF in String C)
	M(2,1,4)	-	-	-	-	-	19.3	2311	46.3	52.2	0	-	-	-	-	-	4 (OCF in String D)
	M(3,1,0)	-	-	-	-	-	-	-	-	-	-	0	1619	187.4	207.3	52.7	0 (No fault in array)
	M(3,1,1)	-	-	-	-	-	-	-		-	-	1713	2.10	3069	3148	2398	1 (OCF in String A)
	M(3,1,2)	-	-	-	-	-	-	-	-	-	-	183	2860	0.2	1.39	35.5	2 (OCF in String B)
	M(3,1,3)	-	-	-	-	-	-	-	-	-	-	31.6	3099	2.95	1.02	66.4	3 (OCF in String C)
	M(3,1,4)	-	-	-	-	-	-	-	-	-	-	62.7	2291	36.9	46.1	0.12	4 (OCF in String D)

Data presented in scientific notation of $x10^{-4}$.

TABLE 6. ***J(F)*** **Values obtained from all the experimental tests conducted on the 4 × 2 PV array.**

		Database Identifier $L(T_L,S_L,F_L)$															
		L(1,1,0)	*L(1,1,1)*	*L(1,1,2)*	*L(1,1,3)*	*L(2,1,4)*	*L(2,1,0)*	*L(2,1,1)*	*L(2,1,2)*	*L(2,1,3)*	*L(2,1,4)*	*L(3,1,0)*	*L(3,1,1)*	*L(3,1,2)*	*L(3,1,3)*	*L(3,1,4)*	**Indicator of failure location**
Test identifier $M(T_M,S_M,F_M)$	*M(1,1,0)*	5.2	1864	140.4	197.6	49.1	-	-	-	-	-	-	-	-	-	-	0 (No fault in array)
	M(1,1,1)	1796	2.25	3195	3450	2671	-	-	-	-	-	-	-	-	-	-	1 (OCF in String A)
	M(1,2,2)	216.3	3091	0.3	2.6	29.2	-	-	-	-	-	-	-	-	-	-	2 (OCF in String B)
	M(1,1,3)	243	3189	2.1	0.5	39.5	-	-	-	-	-	-	-	-	-	-	3 (OCF in String C)
	M(1,2,4)	63.2	2385	38.3	70.5	1.8	-	-	-	-	-	-	-	-	-	-	4 (OCF in String D)
	M(2,1,0)	-	-	-	-	-	6.3	1694	188.5	200.2	50.9	-	-	-	-	-	0 (No fault in array)
	M(2,1,1)	-	-	-	-	-	2048	2.49	3188	3236	2488	-	-	-	-	-	1 (OCF in String A)
	M(2,1,2)	-	-	-	-	-	115.9	2964	0.1	0.7	37.8	-	-	-	-	-	2 (OCF in String B)
	M(2,1,3)	-	-	-	-	-	170.8	3220	3.4	2	71.4	-	-	-	-	-	3 (OCF in String C)
	M(2,1,4)	-	-	-	-	-	19.3	2311	46.3	52.2	0	-	-	-	-	-	4 (OCF in String D)
	M(3,1,0)	-	-	-	-	-	-	-	-	-	-	0	1619	187.4	207.3	52.7	0 (No fault in array)
	M(3,1,1)	-	-	-	-	-	-	-		-	-	1713	2.10	3069	3148	2398	1 (OCF in String A)
	M(3,1,2)	-	-	-	-	-	-	-	-	-	-	183	2860	0.2	1.39	35.5	2 (OCF in String B)
	M(3,1,3)	-	-	-	-	-	-	-	-	-	-	31.6	3099	2.95	1.02	66.4	3 (OCF in String C)
	M(3,1,4)	-	-	-	-	-	-	-	-	-	-	62.7	2291	36.9	46.1	0.12	4 (OCF in String D)

Data presented in scientific notation of $x10^{-4}$.

the median values obtained for each of the possible cases of failure in a string are different.

The DFT magnitudes of the simulated results are greater than those obtained in the experimental tests, which is due to the electrical characteristics of the simulated modules, which are different from those in the experimental modules. However, this does not interfere with the fault location, demonstrating that the method can be used in modules with different electrical characteristics.

Tables 5 and 6 show the J(F) values, which were obtained by applying the classifier and indicator to the experimentally obtained median reference values obtained via the learning and monitoring modes for the 4 × 1 and 4 × 2 PV arrays, respectively. Tables 5 and 6 show that the F value, obtained from the lowest J(F) value from each experimental test, agrees with the open circuit failure location found in the evaluated test (FM). Several tests for the 4 × 1 and 4 × 2 PV arrays were performed to validate the method.

Likewise, several tests for 4 × 3 were performed to demonstrate the scalability of the method. In all tests, similar results were obtained. The method correctly indicated the open circuit fault location in a string, and it can be applied to photovoltaic arrays of different sizes.

IX. CONCLUSIONS

The used of pulsed light on one PV module enables a forward bias voltage to be input into a PV array when is operated under dark conditions and without the disconnection of or any modification to the PV array. The changes in the AC frequency component of the output voltage array enable the detection of the PV array condition.

The presence of an open circuit fault in a series-parallel PV array operated under dark conditions and forward bias voltage generates an increase in the total dynamic impedance. As a result, this increase also generates an increase in the AC component of the array output voltage, which enables

fault detection. However, variability in the module impedances also generates variations in the total dynamic impedances. The results of both phenomena can be combined in order to locate the fault.

Here, the use of DFT and the median value obtained are shown to enable the extraction of important information that facilitates the location of open circuit fault in the string of a PV array.

In all tests, the experimental results showed 100% detection and location of the string with an open circuit fault. The simulation demonstrates that the presence of a failure in each string generates changes in the amplitude of the component frequency of 6 kHz, which is the frequency of the light signal applied to one module of the PV array. These results agree with the results obtained from the experimental array, validating the effectiveness of the method.

Moreover, it is noteworthy that the size of the PV array, the temperature and the different electrical characteristics of the modules used do not interfere with condition detection and failure location. The methodology presented here can be applied in a real plant, because of the low voltage it will generate. This is possible because the PV plant will be operated under dark conditions using pulsed light as the light source. A significant contribution of the method is that it operates in conditions of darkness (irradiance less than 1 W/m^2), thus taking advantage of the time of no natural operation (night) to assess the conditions of the photovoltaic array. Additionally, it is important to highlight that the proposed method does not require sensors or expensive and specialized equipment, nor does it require the disconnection of or any modification to the PV array. Furthermore, the use of this method avoids the risk of electrical shock during fault monitoring. For all the above reasons, it can be concluded that the proposed method is reliable, simple, fast, low-cost, low computing power and safe in comparison with other reported methods. The estimated implementation cost is approximately USD 1000.

REFERENCES

[1] M. Banavar, H. Braun, S. T. Buddha, V. Krishnan, A. Spanias, S. Takada, T. Takehara, C. Tepedelenlioglu, and T. Yeider, "Signal processing for solar array monitoring, fault detection, and optimization (synthesis lectures on power electronics)," vol. 3, no. 1, San Rafael, CA, USA: Morgan & Claypool, J. Hudgins, Ed., 2012, pp. 1–95. doi: 10.2200/S00425ED1V01Y201206PEL004.

[2] A. Mellit, G. M. Tina, and S. A. Kalogirou, "Fault detection and diagnosis methods for photovoltaic systems: A review," *Renew. Sustain. Energy Rev.*, vol. 91, pp. 1–17, Aug. 2018. doi: 10.1016/j.rser.2018.03.062.

[3] M. K. Alam, F. Khan, J. Johnson, and J. Flicker, "A comprehensive review of catastrophic faults in PV arrays: Types, detection, and mitigation techniques," *IEEE J. Photovolt.*, vol. 5, no. 3, pp. 982–997, May 2015. doi: 10.1109/JPHOTOV.2015.2397599.

[4] G. M. Tina, F. Cosentino, and C. Ventura, "Monitoring and diagnostics of photovoltaic power plants," in *Renewable Energy in the Service of Mankind*, vol. 2, A. Sayigh, Ed. Cham, Switzerland: Springer, 2016, pp. 505–516. doi: 10.1007/978-3-319-18215-5_45.

[5] P. Ducange, M. Fazzolari, B. Lazzerini, and F. Marcelloni, "An intelligent system for detecting faults in photovoltaic fields," in *Proc. ISDA*, Cordoba, Spain, Nov. 2011, pp. 1341–1346. doi: 10.1109/ISDA.2011.6121846.

[6] W. Chine and A. Mellit, "ANN-based fault diagnosis technique for photovoltaic stings," in *Proc. ICEE-B*, Boumerdes, Algeria, Oct. 2017, pp. 1–4. doi: 10.1109/ICEE-B.2017.8192078.

[7] S. Vergura, G. Acciani, V. Amoruso, and G. Patrono, "Inferential statistics for monitoring and fault forecasting of PV plants," *Presented IEEE ISIE*, Cambridge, U.K., Jun./Jul. 2008, pp. 2414–2419. doi: 10.1109/ISIE.2008.4677264.

[8] K.-H. Chao, P.-Y. Chen, M.-H. Wang, and C.-T. Chen, "An intelligent fault detection method of a photovoltaic module array using wireless sensor networks," *Int. J. Distrib. Sensor Netw.*, vol. 10, no. 5, May 2014, Art. no. 540147. doi: 10.1155/2014/540147.

[9] N. Gokmen, E. Karatepe, S. Silvestre, B. Celik, and P. Ortega, "An efficient fault diagnosis method for PV systems based on operating voltage-window," *Energy Conver. Manage.*, vol. 73, pp. 350–360, Sep. 2013. doi: 10.1016/j.enconman.2013.05.015.

[10] Y. Zhao, B. Lehman, R. Ball, J. Mosesian, and J.-F. de Palma, "Outlier detection rules for fault detection in solar photovoltaic arrays," *Presented 28th Annu. IEEE Appl. Power Electron. Conf. Exposit. (APEC)*, Long Beach, CA, USA, Mar. 2013, pp. 2913–2920. doi: 10.1109/APEC.2013.6520712.

[11] Y. Zhao, R. Ball, J. Mosesian, J.-F. De Palma, and B. Lehman, "Graph-based semi-supervised learning for fault detection and classification in solar photovoltaic arrays," *IEEE Trans. Power Electron.*, vol. 30, no. 5, pp. 2848–2858, May 2015. doi: 10.1109/TPEL.2014.2364203.

[12] G. Chen, P. Lin, Y. Lai, Z. Chen, L. Wu, and S. Cheng, "Location for fault string of photovoltaic array based on current time series change detection," *Energy Procedia*, vol. 145, pp. 406–412, Jul. 2018. doi: 0.1016/j.egypro.2018.04.06.

[13] E. Garoudja, F. Harrou, Y. Sun, K. Kara, A. Chouder, and S. Silvestre, "Statistical fault detection in photovoltaic systems," *Sol. Energy*, vol. 150, pp. 485–499, Jul. 2017. doi: 0.1016/j.solener.2017.04.

[14] F. Harrou, Y. Sun, B. Taghezouit, A. Saidi, and M.-E. Hamlati, "Reliable fault detection and diagnosis of photovoltaic systems based on statistical monitoring approaches," *Renew. Energy*, vol. 116, pp. 22–37, Feb. 2018. doi: 0.1016/j.renene.2017.09.048..

[15] N. Gokmen, E. Karatepe, B. Celik, and S. Silvestre, "Simple diagnostic approach for determining of faulted PV modules in string based PV arrays," *Sol. Energy*, vol. 86, no. 11, pp. 3364–3377, Nov. 2012. doi: 10.1016/j.solener.2012.09.007.

[16] K. A. Saleh, A. Hooshyar, E. F. El-Saadany, and H. H. Zeineldin, "Voltage-based protection scheme for faults within utility-scale photovoltaic arrays," *IEEE Trans. Smart Grid*, vol. 9, no. 5, pp. 4367–4382, Sep. 2018.doi: 10.1109/TSG.2017.2655444.

[17] A. Khoshnami and I. Sadeghkhani, "Sample entropy-based fault detection for photovoltaic arrays," in *IET Renew. Power Gener.*, vol. 12, no. 16, pp. 1966–1976, Dec. 2018. doi: 10.1049/iet-rpg.2018.5220.

[18] T. Takashima, J. Yamaguchi, K. Otani, K. Kato, and M. Ishida, "Experimental studies of failure detection methods in PV module strings," *Presented IEEE 4th WCPEC*, Waikoloa, HI, USA, May 2006, pp. 2227–2230. doi: 10.1109/WCPEC.2006.279952.

[19] L. Schirone, F. P. Califano, and M. Pastena, "Fault detection in a photovoltaic plant by time domain reflectometry," *Progr. Photovolt. Res. Appl.*, vol. 2, no. 1, pp. 35–44, Jan.,1994. doi: 10.1002/pip.4670020106..

[20] T. Takashima, J. Yamaguchi, and M. Ishida, "Fault detection by signal response in PV module strings," *Presented 33rd IEEE PVSC*, San Diego, CA, USA, May 2008, pp. 1–5. doi: 10.1109/PVSC.2008.4922843.

[21] L. Schirone, F. P. Califano, U. Moschella, and U. Rocca, "Fault finding in a 1 MW photovoltaic plant by reflectometry," in *Proc. 1st WCPEC*, Waikoloa, HI, USA, Dec. 1994, pp. 846–849. doi: 10.1109/WCPEC.1994.520093.

[22] T. Takashima, J. Yamaguchi, and M. Ishida, "Disconnection detection using earth capacitance measurement in photovoltaic module string," *Prog. Photovolt. Res. Appl.*, vol. 16, no. 8, pp. 669–677, Dec. 2008. doi: 10.1002/pip.860.

[23] T. Takashima, J. Yamaguchi, K. Otani, T. Oozeki, K. Kato, and M. Ishida, "Experimental studies of fault location in PV module strings," *Solar Energy Mater. Solar Cells*, vol. 93, nos. 6–7, pp. 1079–1082, Jun. 2009. doi: 10.1016/j.solmat.2008.11..

[24] P. Tavner, L. Ran, J. Penman, and H. Sedding, *Condition Monitoring of Rotating Electrical Machines*, 2nd ed. London, U.K.: Institution of Engineering and Technology, 2008.

[25] J. C. Jáuregui, J. R. Reséndiz, S. Thenozhi, T. Szalay, Á. Jacsó and M. Takács, "Frequency and time-frequency analysis of cutting force and vibration signals for tool condition monitoring," *IEEE Access*, vol. 6, pp. 6400–6410, 2018. doi: 10.1109/ACCESS.2018.2797003.

[26] J. Johnson, S. Kuszmaul, W. Bower, and D. Schoenwald, "A using PV module and line frequency response data to create robust Arc fault detectors," *Presented 26th Conf. EU PVSEC*, Hamburg, Germany, Sep. 2011, pp. 3745–3750. doi: 10.4229/26thEUPVSEC2011-4AV.3.24.
[27] H. S. Rauschenbach, *Solar Cell Array Design Handbook*, 1st ed. New York, NY, USA: Springer, 1980. doi: 10.1007/978-94-011-7915-7.
[28] M. S. Suresh, "Measurement of solar cell parameters using impedance spectroscopy," *Sol. Energy Mater. Sol. Cells*, vol. 43, no. 1, pp. 21–28, Aug. 1996. doi: 10.1016/0927-0248(95)00153-0.
[29] A. Luque and S. Hegedus, *Handbook of Photovoltaic Science and Engineering*, 2nd Ed. Hoboken, NJ, USA: Wiley, 2010.
[30] D. Chenvidhya, K. Kirtikara, and C. Jivacate, "Dynamic impedance characterization of solar cells and PV modules based on frequency and time domain," in *Trends in Solar Energy Research*. New York, NY, USA: Nova Science, 2006, pp. 21–45.
[31] J. Johnson, D. Schoenwald, S. Kuszmaul, J. Strauch, and W. Bower, "Creating dynamic equivalent PV circuit models with impedance spectroscopy for arc fault modeling," *Presented 37th IEEE Photovoltaic Spec. Conf.*, Seattle, WA, USA, Jun. 2011, pp. 002328–002333. doi: 10.1109/PVSC.2011.6186419.

PERLA-YAZMÍN SEVILLA-CAMACHO received the B.S. degree and the master's degree in electronics engineering from the Instituto Tecnológico de Celaya (ITTC), Guanajuato, Mexico, and the Ph.D. degree in engineering from the Universidad Autónoma de Querétaro (UAQ), Querétaro, Mexico, in 2012. Since 2007, she has been a Professor with the University Politécnica of Chiapas (UPChiapas). Her current research interests include experimental and theoretical investigation of fault detection and condition monitoring applied to mechanical systems, and renewable energy systems. She is a member of the National System of Researchers (SNI) in Mexico.

MARCO-ANTONIO ZUÑIGA-REYES received the B.S. degree in electronics engineering from the Instituto Tecnológico de Tuxtla Gutiérrez (ITTG), Mexico, in 1997, and the master's degree in renewable energy from the Universidad Politécnica de Chiapas (UPChiapas). He is currently pursuing the Ph.D. degree.

JOSE-BILLERMAN ROBLES-OCAMPO received the B.S degree and the master's degree in mechanical engineering and the Ph.D. degree in engineering, in 2003, 2007, and 2012, respectively. He has been a Professor/Researcher with the Universidad Politécnica de Chiapas (UPChiapas), since 2012. His research interests include renewable energy, fault detection in dynamics systems, and CNC machines. He is a member of the National System of Researchers (SNI) in Mexico.

ROGER CASTILLO-PALOMERA received the B.S. degree in physics from the Universidad Juárez Autónoma de Tabasco, and the M.Sc. degree in energy engineering (solar-photovoltaic area) and the Ph.D. degree from the Universidad Nacional Autónoma de México (UNAM). Since 2008, he has been a Professor/Researcher with the Universidad Politécnica de Chiapas (UPChiapas), where he is currently the Director of the Energy Engineering Career and the Coordinator of the Master in Renewable Energy. His research interests include the study and characterization of new materials for solar applications, and the implementation of photovoltaic and thermal technologies. He is a member of the National System of Researchers and the State System.

JESÚS MUÑIZ received the Ph.D. degree in materials science and engineering from the Universidad Nacional Autónoma de México (UNAM), in 2008. He held a postdoctoral position with the Chemistry Department, Universidad de Helsinki, in 2009. He was a Professor with the Energy Engineering Program, Universidad Politécnica de Chiapas (UPChiapas), from 2010 to 2014. He has been a Senior Researcher with the Instituto de Energías Renovables, UNAM, since 2014. His research interest includes computational simulation of materials for energy conversion and storage. He has been an active member of the National System of Researchers (Mexico), since 2011.

JUVENAL RODRÍGUEZ-RESÉNDIZ (SM'13) received the Ph.D. degree from the Universidad Autónoma de Querétaro (UAQ), Mexico, in 2010. He was a Visiting Professor with the Universidad de Virginia Occidental (WVU), in 2012. Since 2008, he has been a Professor with UAQ, where he is currently the Chair of the Engineering Automation Program and the Master in Automation Program and the Director of Technologic Link. He has worked on industrial and academic automation projects for 15 years. He received several awards for his contributions in developing education technology. He is a member of the Mexican Academy of Sciences and the National Research Academy (SNI) in Mexico. He is the past President of the IEEE Querétaro Section.